THE JOURNAL OF PHYSICAL CHEMISTRY B

pubs.acs.org/JPCB Article

Cholesterol Reduces Partitioning of Antifungal Drug Itraconazole into Lipid Bilayers

Published as part of The Journal of Physical Chemistry virtual special issue "Computational and Experimental Advances in Biomembranes".

Chetan Poojari, Agata Zak, Monika Dzieciuch-Rojek, Alex Bunker, Mariusz Kepczynski,* and Tomasz Róg*

Cite This: *J. Phys. Chem. B* 2020, 124, 2139–2148 Read Online

ACCESS | Metrics & More | Article Recommendations | Supporting Information

ABSTRACT: Cholesterol plays a crucial role in modulating the physicochemical properties of biomembranes, both increasing mechanical strength and decreasing permeability. Cholesterol is also a common component of vesicle-based delivery systems, including liposome-based drug delivery systems (LDSs). However, its effect on the partitioning of drug molecules to lipid membranes is very poorly recognized. Herein, we performed a combined experimental/computational study of the potential for the use of the LDS formulation for the delivery of the antifungal drug itraconazole (ITZ). We consider the addition of cholesterol to the lipid membrane. Since ITZ is only weakly soluble in water, its bioavailability is limited. Use of an LDS has thus been proposed. We studied lipid membranes composed of cholesterol, 1-palmitoyl-2-oleoyl-*sn*-glycerol-3-phosphocholine (POPC), and ITZ using a combination of computational molecular dynamics (MD) simulations of lipid bilayers and Brewster angle microscopy (BAM) experiments of monolayers. Both experimental and computational results show separation of cholesterol and ITZ. Cholesterol has a strong preference to orient parallel to the bilayer normal. However, ITZ, a long and relatively rigid molecule with weakly hydrophilic groups along the backbone, predominantly locates below the interface between the hydrocarbon chain region and the polar region of the membrane, with its backbone oriented parallel to the membrane surface; the orthogonal orientation in the membrane could be the cause of the observed separation. In addition, fluorescence measurements demonstrated that the affinity of ITZ for the lipid membrane is decreased by the presence of cholesterol, which is thus probably not a suitable formulation component of an LDS designed for ITZ delivery.

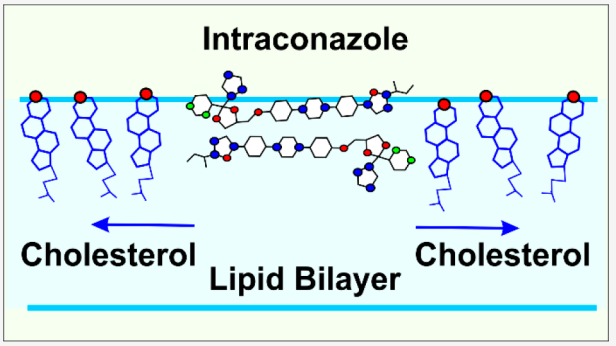

INTRODUCTION

Pharmaceutical nanotechnology, also known as nanomedicine,[1] is the development of nanoscale drug delivery vehicles, also known as nanoparticles. It can be seen as the development of mechanisms to both increase efficacy and reduce toxicity associated with a given drug by targeting the delivery to the desired tissue, through either active or passive means; a specific dose of the drug can thus have an increased efficacy with reduced side effects. The liposome-based delivery system (LDS) is, so far, the most successful form of the nanoparticle, representing more than half of all currently approved nanomedicine-based drug therapies.[2−4] An LDS is composed of a phospholipid membrane formed into an enclosed sac; use of phospholipids and other biocompatible molecules for the membrane possesses the advantage of automatic biocompatibility. As a nanoparticle, the LDS is extremely versatile, it can carry hydrophobic drugs within the membrane[5] or hydrophilic drugs within the internal pocket.[6] Many aspects of the formulation can be altered to tune the properties of the LDS. A subset of the phospholipids can have polymers conjugated to their headgroup to create a protective polymer corona; poly(ethylene glycol) is currently the gold standard in this capacity. Other amphiphilic biocompatible molecules can be added to the membrane to tune its properties; the most commonly used of these is cholesterol (Chol).

A common component of the LDS formulation, Chol is present in 9 out of 15 clinically approved LDS-based drugs and an additional 12 products currently in clinical trials.[7] As an important component that modulates the properties of

Received: November 25, 2019
Revised: January 28, 2020
Published: February 26, 2020

https://dx.doi.org/10.1021/acs.jpcb.9b11005
J. Phys. Chem. B 2020, 124, 2139–2148

biomembranes, Chol can play the same role in an LDS; it has the ability to modify the physical properties of a lipid membrane (for extensive reviews, see, e.g., refs 8−12). For example, the presence of Chol can increase the mechanical strength of the lipid bilayer[13−16] leading to both increased stability and decreased passive permeability to water, ions, and small polar molecules, e.g., glucose and drugs.[17−22] Liposomes with a high Chol concentration are also biocompatible since Chol is present in a high concentration in biomembranes; in particular, the cell membrane of erythrocytes has a Chol level as high as 50%.[23] There are, however, also disadvantages regarding the use of Chol; for example, Chol is prone to oxidation.[24,25] Not surprising, oxidized derivatives of cholesterol have been found in a wide range of cosmetics,[26] processed foods,[27] and liposomal pharmaceutics.[28]

The drug itraconazole (ITZ) (Figure 1), used to treat mycotic infections, is an ideal candidate for delivery via LDSs.

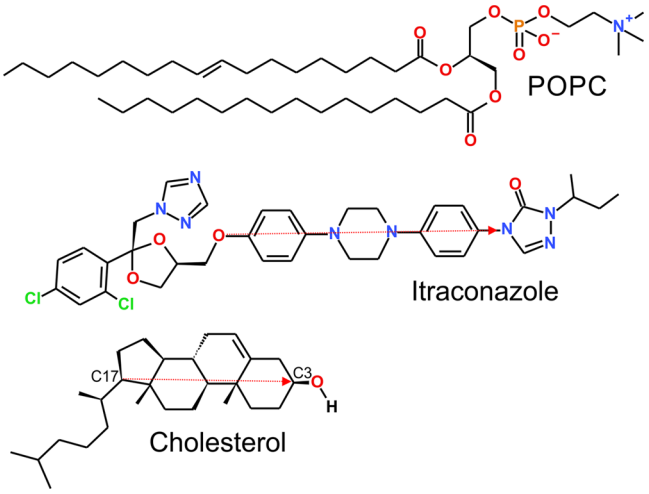

Figure 1. Chemical structure of molecules used in this study. Red arrows show long axes of the molecules. Vertical black-dotted lines show the fragments used for center of mass calculations (see Figure 9).

With a solubility of only 1 ng/mL,[29] ITZ bioavailability is a severe problem in terms of its efficacy. The incorporation of water insoluble drugs into an LDS has seen considerable success as a strategy to solve this problem.[30] In fact, the incorporation of ITZ into multilamellar vesicles, a form of LDS, was shown to increase efficacy in the treatment of pneumonia in comparison to the same drug provided orally, dissolved by PEG or incorporated into cyclodextrin.[31] In previous work, we have shown that ITZ can be incorporated into conventional and PEGylated liposomes at a concentration level of up to 15 mol %.[32] We have now, as a next step, investigated the effect of the addition of Chol into an LDS that already carries ITZ using a combined analysis platform that includes both computational molecular dynamics (MD) simulations of the LDS membrane and Brewster angle microscopy (BAM) of monolayers in a Langmuir balance (LB). Both computational and experimental results are in agreement and present a surprising result: ITZ and cholesterol do not coexist in the membrane; rather, they separate within the membrane. The separation of ITZ and Chol is the reason for the lower affinity of the drug for the lipid membrane containing Chol, as shown by fluorescence measurements. We thus propose that our results indicate that inclusion of Chol into the lipid membrane is probably not beneficial for the case of ITZ delivery.

MATERIALS AND METHODS

Materials. Synthetic 1-palmitoyl-2-oleoyl-*sn*-glycero-3-phosphocholine (POPC), cholesterol (Chol), and itraconazole (ITZ) were received from Sigma-Aldrich. Methanol and chloroform were obtained from Sigma-Aldrich (HPLC grade, ≥99.9%). The ultrapure Milli-Q water, used in the experiments, had a surface tension of 72.6 mN/m (at 20 °C) and a resistivity of 18 MΩ cm.

Langmuir Balance and Brewster Angle Microscopy (BAM) Measurements. The measurements were performed using a KSV 2000 Langmuir trough (KSV Instruments Ltd., Helsinki, Finland) equipped with an ultraBAM (Accurion GmbH, Goettingen, Germany) microscope, as previously described.[32,33] The BAM microscope was equipped with a 50 mW laser emitting p-polarized light at 658 nm, a 10× objective, and a CCD camera. The spatial resolution of the BAM images was 2 μm. To prepare stock solutions, POPC and Chol were dissolved in chloroform/methanol (4:1 v/v), and ITZ was dissolved in chloroform. Phosphate buffer (pH 7.4) was used as the subphase. All experiments were repeated at least twice to ensure consistent results. Surface pressure−area (π−A) isotherms were reproducible within an error of ±0.02 nm^2 molecules^{-1}.

Liposome-Binding Constant Measurements. POPC and POPC/Chol 4:1 liposomes were prepared by sonication using the modified procedure described previously.[34] Briefly, POPC and Chol were dissolved in chloroform to form stock solutions. The appropriate volumes of the stock solutions were combined in a volumetric flask, and chloroform was evaporated under vacuum. Water was added to reach a lipid concentration of 2.5 mg/mL, and the sample was vortex mixed for several minutes. The lipid dispersion was subjected to five freeze−thaw cycles from liquid nitrogen temperature to 60 °C and sonication at ice temperature for 10 min using a titanium tip SONICS VC 130 sonicator. Binding constants (K_b's) of the drug to liposomes were determined using a fluorescence titration technique.[35] Fluorescence spectra were measured using a LS-55 PerkinElmer fluorimeter.

Molecular Dynamics (MD) Simulations. MD simulations were performed for four systems containing hydrated lipid bilayers composed of POPC and Chol (20 mol %) (the POPC/Chol bilayer) and ITZ, at a concentration of one

Table 1. Composition of Lipid Bilayers Used in This Study

system	no. of ITZ	no. of POPC	no. of Chol	no. of water	no. of Na ions	no. of Cl ions	no. of repeats	simulation time (ns)
S1	1	102	26	6940	37	37	3	3000
S1*	1	102	26	3356	24	24	3	3000
S2	9	918	234	62460	333	333	1	1000
S3		918	234	34362	216	216	1	2000

https://dx.doi.org/10.1021/acs.jpcb.9b11005
J. Phys. Chem. B 2020, 124, 2139−2148

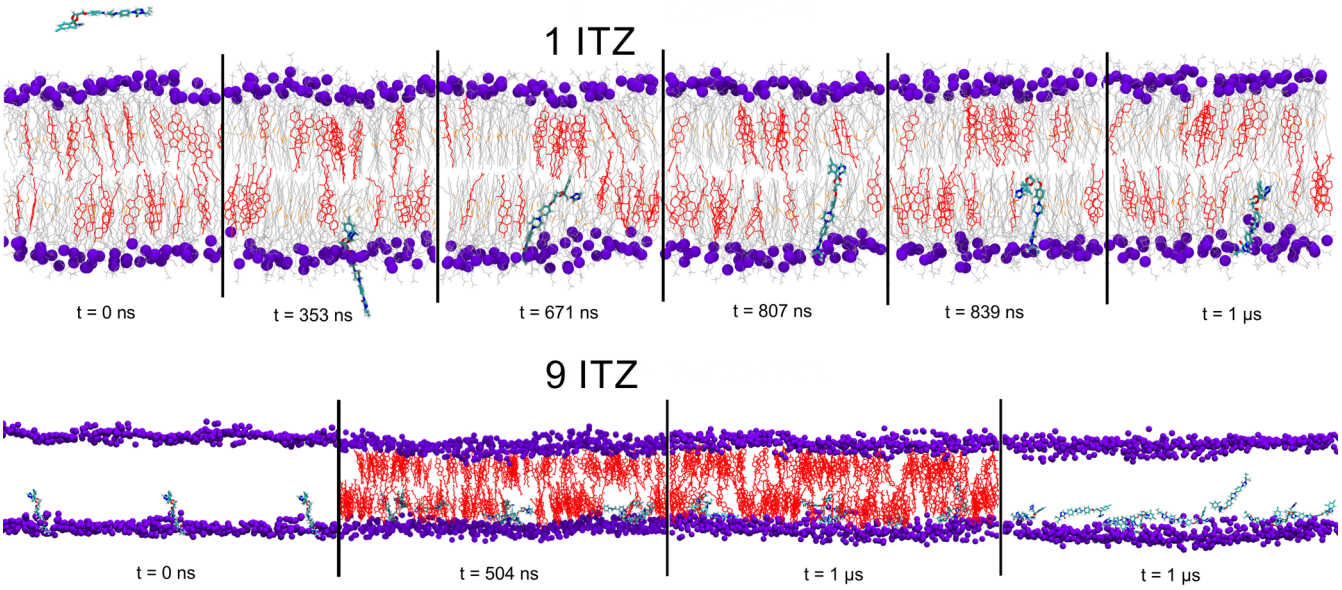

Figure 2. Snapshots of simulated systems at several time windows: ITZ molecules are shown in standard colors, cholesterol is shown in red, POPC phosphate groups are shown as violet spheres, and POPC acyl tails are shown in gray. The figure was prepared using VMD software.[51]

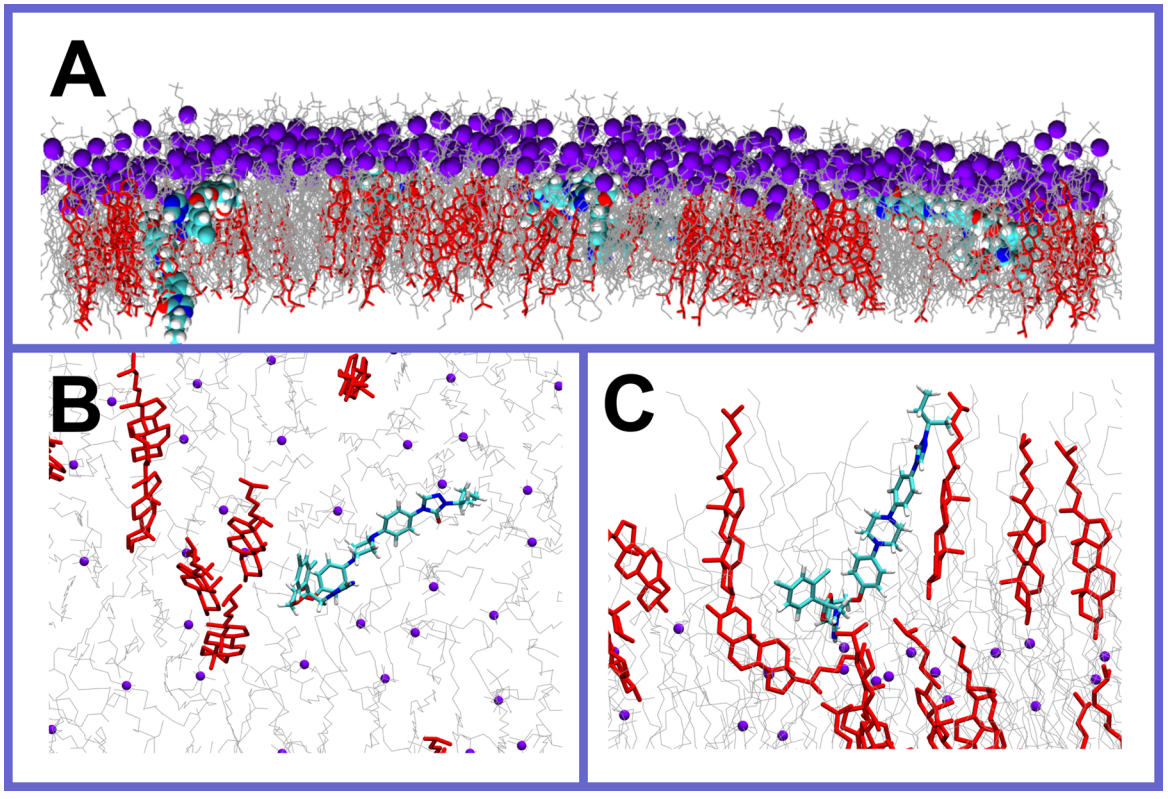

Figure 3. Snapshot of the one leaflet containing ITZ (A), and close views of an ITZ molecule in system **S2** from top (B) and side (C). Cholesterol is shown in red, ITZ in blue with red oxygens and white hydrogens, POPC in gray, and POPC phosphorus atoms in dark blue.

molecule per 128 lipids. Detailed compositions of all systems are given in Table 1. In system **S1**, a single ITZ molecule was inserted into the water phase and allowed to spontaneously insert into the lipid bilayer. System **S2** was constructed by replicating the frame of system **S1** three times over periodic boundary conditions in the bilayer plane (*XY*) to create a lipid bilayer nine times larger than that of **S1**. System **S1*** was constructed from model **S1** by decreasing the number of water molecules. A physiological salt concentration (140 mM of NaCl) was used. The results were averaged over simulated replicates and molecules present in the bilayer.

To parametrize all molecules and ions, we used the OPLS-AA force field.[36−38] We used lipid models derived in our prior studies[39−42] (molecular topologies of POPC and Chol are provided in Supporting Materials of ref 40). Partial charges for the ITZ molecule were derived in the previously published work.[32] To model water we used the TIP3 parameter set.[43] All simulations were performed using the GROMACS software

https://dx.doi.org/10.1021/acs.jpcb.9b11005
J. Phys. Chem. B 2020, 124, 2139−2148

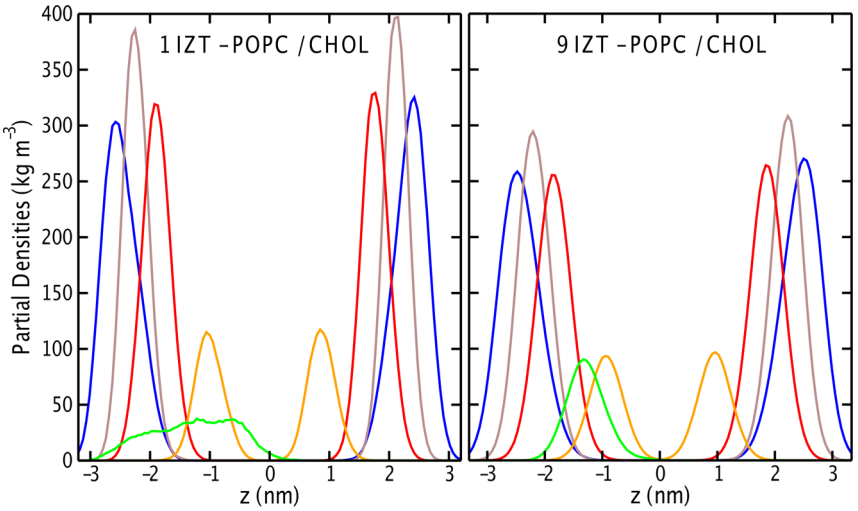

Figure 4. Mass density profiles of ITZ (green lines) and the selected POPC atoms (nitrogens, blue lines; phosphorus, gray lines; carbonyl oxygens, red lines; double bond atoms, orange lines) along the bilayer normal as averaged over the last 500 ns of the simulations.

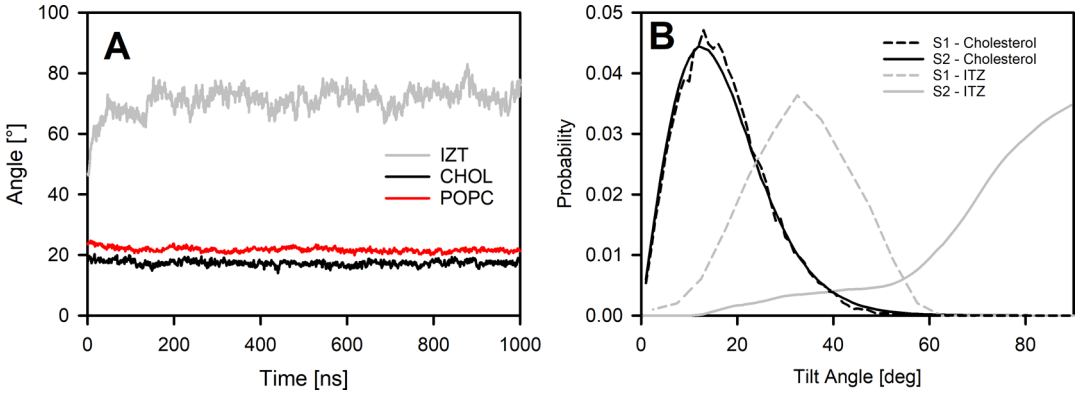

Figure 5. (A) Time development of tilt angles for ITZ (gray line), Chol (black line), and POPC *sn*1 tail (red line) in system **S2**. (B) Probability distributions of the angles between the vectors representing long axes of the Chol and ITZ molecules (see Figure 1) and the bilayer normal in systems **S1** (dashed lines) and **S2** (solid lines) over the last 600 ns of the trajectories. The data were averaged over all Chol or ITZ molecules present in the system.

package.[44] The LINCS algorithm was used to maintain covalent bond lengths between hydrogens and heavy atoms, allowing for a 2 fs time step.[45] Simulations were performed at constant temperature (300 K) and pressure (1 atm). Temperature and pressure were controlled using the Nose–Hoover[46,47] and Parinello–Rahman[48] algorithms, respectively. The temperature of solute and solvent were controlled independently, and semi-isotropic pressure coupling was used. The long-range electrostatic interactions were calculated using Particle-Mesh-Ewald algorithm with a real space cutoff of 1 nm.[49,50] The neighbor lists were updated every 10 steps.

RESULTS AND DISCUSSION

MD Simulations. Figure 2 shows snapshots of the systems taken at various simulation times. For the case of system **S1**, the ITZ molecule, placed initially in the water phase, entered the membrane after approximately 350 ns of the simulation. Insertion was observed in two out of the six replicas ,and partial insertion was observed in only one replica. For comparison, in our previous studies using a pure POPC bilayer, all ITZ molecules entered the bilayer after less than 450 ns.[32] This observation is consistent with the known reduction in permeability of the bilayer containing Chol.[9] On the other hand, the insertion process is similar for both POPC and POPC/Chol bilayers. During insertion, ITZ is oriented perpendicular to the bilayer surface. The difference lies in the ITZ orientation after insertion: in the POPC bilayer, the drug molecules orient their long axis parallel to the bilayer surface, while in the POPC/Chol membrane, ITZ molecules remain perpendicular to the membrane surface.

For the case of system **S2**, nine ITZ molecules were partially inserted into the bilayer at the beginning of the simulation and separated from each other (Figure 2). During the simulation, all ITZ molecules fully entered the bilayer core. Although the drug/lipid ratio of systems **S1** and **S2** is identical, the behavior of ITZ in these two systems is significantly different. In system **S2**, the drug molecules adopt an orientation parallel to the bilayer surface, similar to the behavior of ITZ in the pure POPC bilayer (Figure 3). In addition, the ITZ molecules form aggregates of three molecules, and the drug tends to accumulate in Chol-depleted regions (Figure 3).

The qualitative differences in the behavior of the ITZ molecules in the two systems (**S1** and **S2**) can be attributed either to the limited size of the bilayer in system **S1** or to the need for the collective action of ITZ molecules to form local clusters oriented parallel to the bilayer surface. Thus, the

https://dx.doi.org/10.1021/acs.jpcb.9b11005
J. Phys. Chem. B 2020, 124, 2139–2148

behavior of ITZ molecules in system **S1** would be representative of the highly diluted system where isolated ITZ molecules adopt the orientation of cholesterol molecules. On the other hand, the simulations of system **S2** clearly demonstrate a tendency of ITZ molecules to aggregate even at low concentrations in Chol-containing lipid bilayers. The cause of ITZ aggregation in the lipid bilayer is probably the drug−Chol separation, which significantly reduces the volume available for the drug in cholesterol-containing membranes. As a result, the drug concentration increases locally.

Figures 4 and 5 provide quantitative results regarding the location and orientation of ITZ in the lipid bilayers. Figure 4 shows the density profiles of ITZ and selected POPC atoms. In system **S2**, ITZ locates preferentially between the headgroup and the double bonds in the *sn*2 chain of POPC with the maximum at 1.4 nm from the bilayer center. In system **S1**, ITZ spreads over the entire leaflet, reflecting its orientation parallel to the membrane normal. Figure 5 shows time development and the distribution of the angles of the long molecular axes of Chol and ITZ. The long axis of Chol molecules makes an average angle of 17.2 ± 0.8° with the bilayer normal. Thus, Chol adopts an orientation approximately parallel to the bilayer normal. The POPC acyl tails have a similar orientation (21.6 ± 0.6°), considering the vector connecting the first and last atom in the *sn*1 chain. In contrast, ITZ molecules predominantly adopt a perpendicular orientation (72 ± 3°), thus parallel to the membrane plane. However, in system **S1**, in which only one ITZ molecule was inserted into the bilayer, the ITZ orientation is more similar to the Chol orientation (the ITZ long axis makes an average angle of 33 ± 5° with the bilayer normal).

To characterize the interactions between ITZ and Chol in the lipid membrane, we calculated the number of contacts between heavy atoms of both molecules. We assumed that a contact occurred when the distance between two (non-hydrogen) atoms was smaller than 0.6 nm. Figure 6 shows

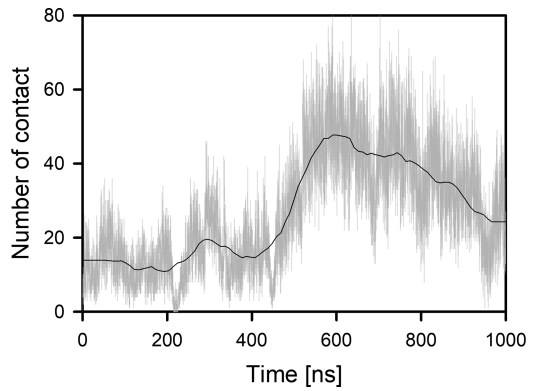

Figure 6. Time development of the number of contacts between atoms of ITZ and Chol. Gray line shows the number of contacts and black line shows running average.

the time development of the number of contacts during the simulation. In the first 400 ns of the simulation, the ITZ−Chol contacts were insignificant. After this time, the number of contacts increased quickly due to the change in the ITZ orientation from parallel to the bilayer normal (initial arrangement) to parallel to the membrane surface. With this arrangement of ITZ, the increase in contact is expected, since ITZ is a long molecule, thus interacting with many lipids while adopting an orientation parallel to the membrane surface. In the next part of the simulation, we observed a decrease in the number of contacts with Chol; this can be interpreted as a sign of separation. This process is, however, not completed within the simulation time.

To further evaluate the ITZ−Chol interactions, we calculated the radial distribution functions (RDFs) for heavy atoms of ITZ and lipids according to the equation

$$\mathrm{RDF} = \frac{V}{N}\left\langle \frac{n(r)}{4\pi r^2 dr} \right\rangle \tag{1}$$

where $n(r)$ is the number of atoms β in the spherical ring with radius r and width dr around the atom α, $4\pi r^2 dr$ is the ring volume, V is the volume of the system, N is the number of atoms, and $\langle\ \rangle$ denotes averaging over time and ensemble. The RDF function (Figure 7) for the ITZ-POPC pair shows a

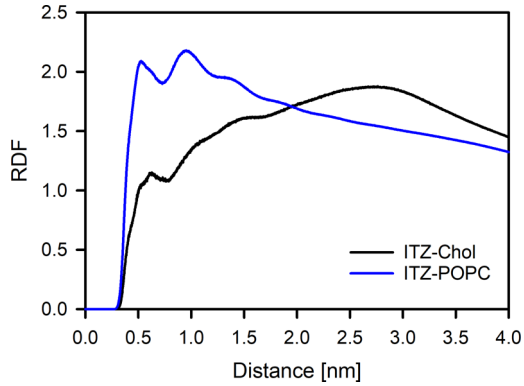

Figure 7. Radial distribution functions (RDFs) for heavy atoms of ITZ with respect to heavy atoms of Chol (black line) and POPC (blue line) calculated for the last 200 ns of the simulations of system **S2**.

narrow maximum located at 0.5 nm, which indicates ITZ preference for interacting with POPC. In the case of a ITZ−Chol pair, the RDF function has a broad maximum centered at 2.8 nm, demonstrating that Chol tends to be located away from the drug. A small maximum can be noticed at approximately 0.6 nm, which indicates that Chol−ITZ interactions are also possible.

To gain insight into the local ITZ impact on POPC properties, we calculated the order parameter, S_{CD}, for the *sn*1 chains of POPC molecules located at the distances up to 1 nm, between 1 and 2 nm, and above 2 nm. The distance was calculated between the center of mass of the acyl tails and the center of mass of three ITZ fragments (see Figure 1) in the plane of the bilayer (only lipids in the same leaflet were included into the calculation). The S_{CD} order parameter is defined as follows:

$$S_{CD} = \left\langle \frac{3}{2}(\cos^2\theta_i) - \frac{1}{2} \right\rangle \tag{2}$$

where θ_i is the angle between the C−H bond of the ith carbon atom and the bilayer normal. The angle brackets mean averaging over time and over appropriate C−H bonds in the bilayer. The S_{CD} parameter profiles along the PA *sn*1 chains (Figure 8) show a decrease in the order of hydrocarbon tails of the lipids in the vicinity of the drug molecules. Therefore, the presence of ITZ in the membrane should increase its fluidity.

https://dx.doi.org/10.1021/acs.jpcb.9b11005
J. Phys. Chem. B 2020, 124, 2139−2148

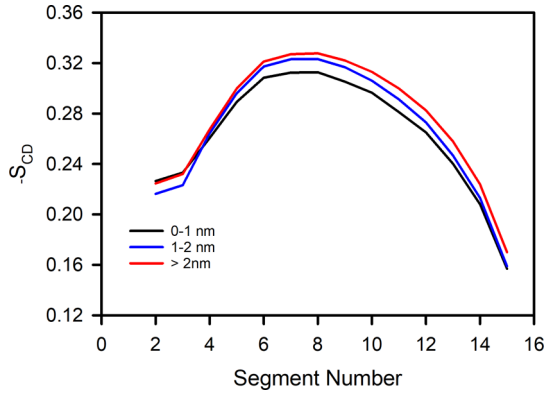

Figure 8. Order parameters (negative values of S_{CD}) for the *sn*1 chain of POPC located at various distances from ITZ calculated for system **S2**.

Monolayer Experiments. The π–A isotherms recorded during compression of the POPC/Chol films and their mixtures with ITZ are presented in Figure 9. To determine if the ITZ effect depends on the Chol content in the model membrane, POPC and Chol were mixed in two different proportions (POPC/Chol = 4:1 and 1:1). The physical state of both POPC/Chol films was determined on the basis of the compression modulus calculated on the basis of the isotherms (Figure S1, the Supporting Information). The calculated values indicate that both monolayers are in the liquid-condensed (LC) phase at larger surface pressures. We introduced a variety of concentrations of ITZ (5, 10, and 15 mol %) into these films.

The addition of ITZ in the investigated concentration range does not drastically affect the position of the isotherms; it however significantly alters their slopes. This indicates that the incorporation of the drug, even at low concentrations, into the POPC/Chol membranes disturbs their structures. The fact that the isotherm slope for ITZ-containing monolayers is less steep than that for the POPC/Chol films indicates that the addition of itraconazole increases the fluidity of the model membranes. This is confirmed by the compression modulus values calculated for the ITZ-containing monolayers (Figure S1, Supporting Information).

The BAM images obtained during the compression of the films are shown in Figure 10. BAM images taken for both two-component (POPC/Chol) monolayers are similar. At low surface pressure (π = 1 mN/m), brighter oval domains of the liquid expanded (LC) phase that coexist with the gaseous (G) phase (darker areas in the images) are visible. When compressing films, the LC domains merge and the LC phase covers the whole interface up to the collapse point. This is reflected in the homogeneous BAM images that confirm the miscibility of POPC and Chol. Our results are consistent with previous studies showing that the excess Gibbs energy of mixing (ΔG_{exc}) for the POPC/Chol binary system is negative for the entire range of monolayer compositions.[52] The only difference that can be noticed between POPC/Chol films is that the LE domains observed for the POPC/Chol 4:1 monolayer are smaller than that for the POPC/Chol (1:1) monolayer. This indicates a higher condensation of the latter monolayer. The observed effect is due to the higher Chol concentration, whose condensing property on phospholipids is well-known.[52,53]

For the case of ternary POPC/Chol/ITZ monolayers, in which the ratio of POPC to Chol was 4:1, their morphology does not change up to 10 mol % of ITZ in the mixed film (BAM images are practically identical to those for the POPC/Chol monolayer, data not shown). The higher content of ITZ (15 mol %), however, causes the condensed phase domains observed at lower surface pressure (π = 1 mN/m) to be smaller than those observed for the two-component POPC/Chol (4:1) monolayer. This confirms that the POPC/Chol/ITZ monolayers have a more liquid character than the POPC/Chol films. In addition, at higher surface pressures ($\pi \geq 10$ mN/m), the monolayers are heterogeneous, and small condensed domains can be observed in the BAM images, suggesting phase separation. ITZ exerts a similar effect on the POPC/Chol 1:1 film; however, the morphology of the monolayer changes at the lower itraconazole content (10 mol %), and monolayers are inhomogeneous over the entire range of surface pressures. Furthermore, at a higher concentration of ITZ (15 mol %), the domains observed at higher surface pressures are very bright. This suggests that multilayer (3-D) structures are present, indicating that, at higher surface pressures, the film-forming molecules (most probably ITZ) are squeezed out from the monolayer. This is

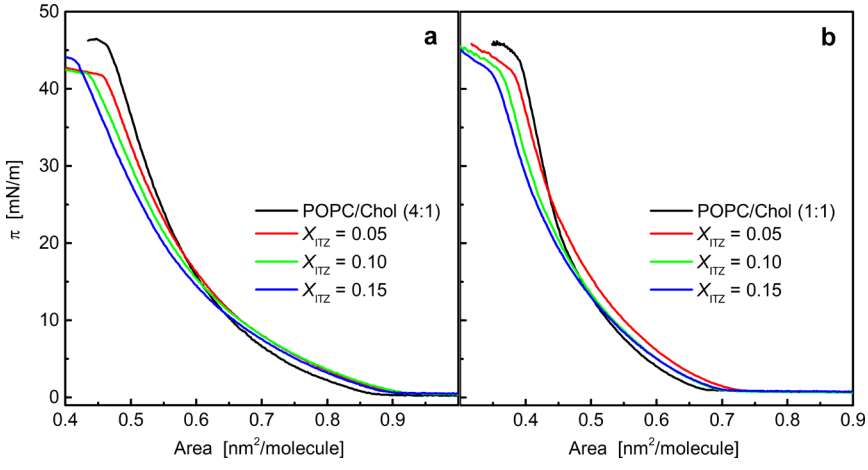

Figure 9. Surface pressure–area (π–A) isotherms for the investigated POPC/Chol (4:1) (a) and POPC/Chol (1:1) (b) monolayers containing different ITZ molar fractions.

https://dx.doi.org/10.1021/acs.jpcb.9b11005
J. Phys. Chem. B 2020, 124, 2139–2148

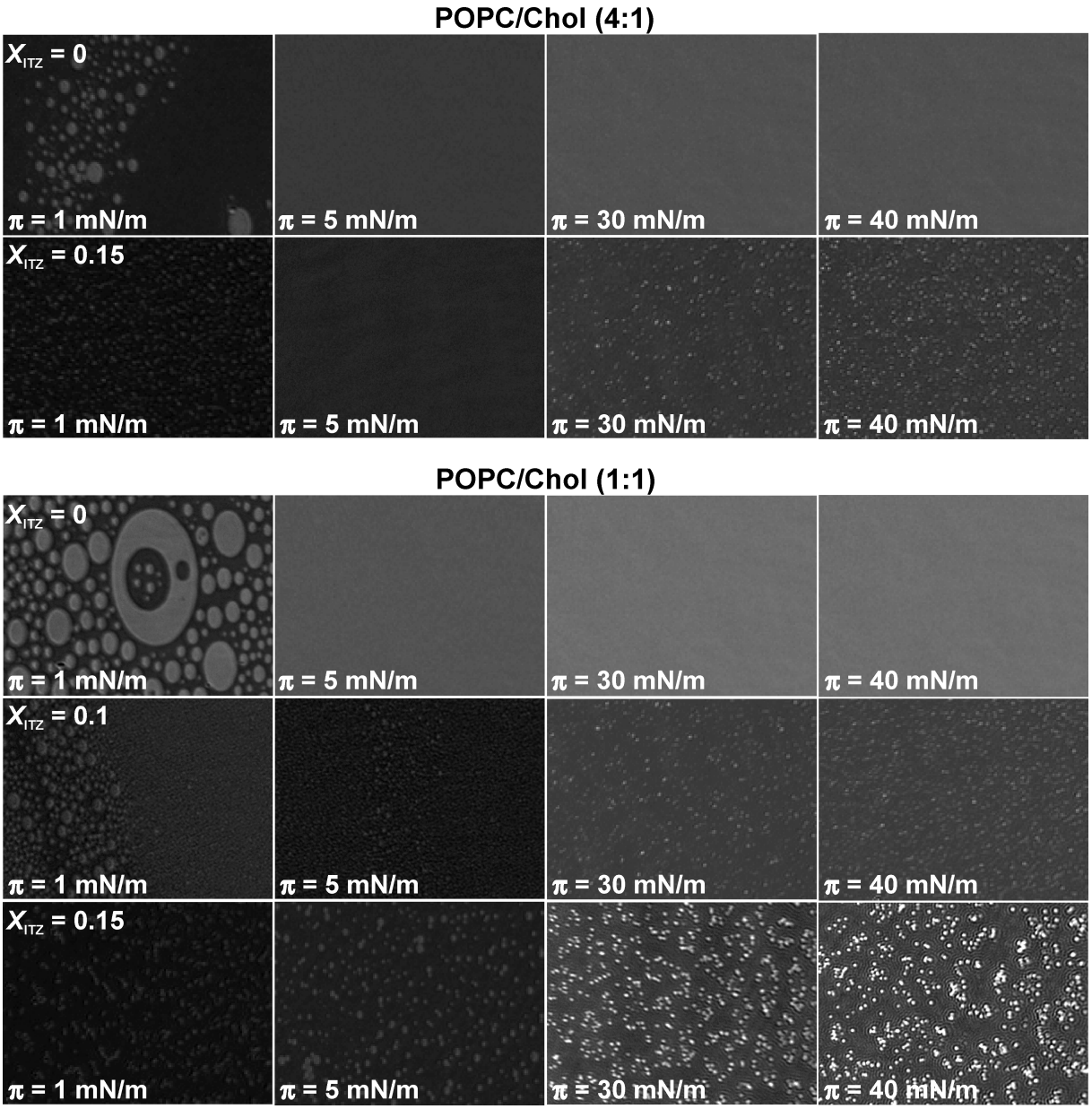

Figure 10. BAM images taken for the investigated films at different stages of compression.

strongly supported by the formation of ITZ clusters observed in the simulations of system **S2**, in which the concentration of the drug was much smaller. The obtained results show that the effect of ITZ on the model membranes depends on the Chol concentration. In our previous studies with the pure POPC bilayer, we showed that the POPC/ITZ monolayers were homogeneous at ITZ concentration levels up to 15 mol % over the entire range of surface pressures.[32] It can therefore be concluded that the higher the level of Chol in the lipid monolayer is, the lower the concentration of ITZ is at which the membrane morphology starts to be disturbed.

Fluorescence Measurements. To assess the effect of Chol on ITZ partitioning between the liposomal and aqueous phases, we determined the so-called binding constant, K_b, defined as[54]

$$K_b = \frac{c_L}{c_w[L]} \tag{3}$$

where c_L and c_w are ITZ concentrations in the liposomal and aqueous phases, respectively. [L] is the lipid concentration in the system. Two sets of samples containing constant ITZ concentration and increasing content of the POPC or POPC/Chol 4:1 liposomes were prepared, and emission spectra were measured. We observed an increase in ITZ fluorescence intensity after the addition of the liposomes. Figure 11 presents a typical dependence of fluorescence intensity (F) and [L] for the ITZ solution titrated with the POPC and POPC/Chol 4:1 vesicles. K_b was determined by fitting the experimental data to the formula[54]

$$F = \frac{F_{init} + F_{comp}K_b[L]}{1 + K_b[L]} \tag{4}$$

where F_{init}, F, and F_{comp} are the fluorescence intensity of the drug measured without lipid, after adding lipid to the concentration [L], and the asymptotic intensity achieved at complete binding, respectively; the fitted line is shown in

https://dx.doi.org/10.1021/acs.jpcb.9b11005
J. Phys. Chem. B 2020, 124, 2139−2148

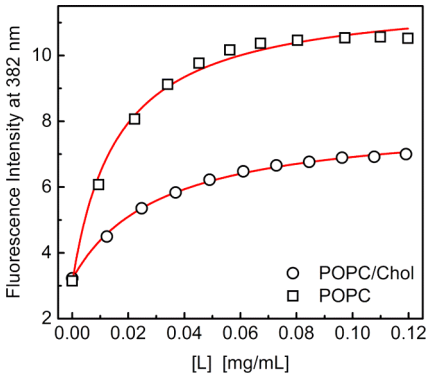

Figure 11. Changes in ITZ fluorescence intensity (c_{ITZ} = 1 μM, λ_{exc} = 270 nm) upon titration with the POPC liposomes (□) and the POPC/Chol 4:1 liposomes (○). The red lines show the best fits to eq 2.

Figure 11. The average binding constants of ITZ to the POPC and POPC/Chol liposomes were found to be 32.0 ± 2.0 and 64.9 ± 5.2 mg mL^{-1}, respectively. These results indicate that the presence of Chol in the lipid membrane can significantly reduce the affinity of the drug for the membrane. This is in line with the results of MD simulations, which show that Chol hinders ITZ penetration into the lipid bilayer.

CONCLUSIONS

Our results clearly demonstrate that Chol and ITZ do not mix in lipid bilayers but rather separate into different domains, thus reducing membrane stability. The orientation of the ITZ molecules in the bilayer results from the shape and distribution of the polar groups in the molecule, and this orientation clashes with that of Chol. Cholesterol is evolutionarily optimized to increase order of the lipids in biological membranes and adopts a slightly tilted orientation toward the normal to the bilayer. This orientation is maintained by its (1) hydroxyl group that locates to the interface between polar and hydrophobic regions, (2) rigid steroid ring that neighbors the ordered section of the lipid tails, and (3) isooctyl tail spanning the most disordered section of the bilayer. While also a rigid molecule, ITZ is, however, longer than the cholesterol molecule or POPC acyl tails; thus, ITZ, in orientation parallel to the bilayer normal, can span the disordered region of the bilayer or even protrude into the opposite leaflet. These two situations are entropically unfavorable due to the ordering effects that result from the presence of a rigid molecule in the highly disordered region of the bilayer. In addition, polar groups are distributed along the entire length of the molecule; thus, in orientation parallel to the bilayer normal, some of them would be buried in the hydrophobic core of the membrane. These two factors lead to the strong preferences of ITZ to locate to the interface between the hydrocarbon chain region and the polar region and then orient parallel to the membrane surface. The drug−Chol separation in the lipid bilayer strongly affects ITZ accumulation in Chol-containing liposomes. The presence of Chol causes the membrane volume available for the drug to be significantly reduced. As a result, at higher concentrations the drug molecules either aggregate within the membrane or are expelled from it entirely.

ASSOCIATED CONTENT

Supporting Information

The Supporting Information is available free of charge at https://pubs.acs.org/doi/10.1021/acs.jpcb.9b11005.

Additional figure showing compression modulus vs surface pressure and the compression modulus calculation (PDF)

AUTHOR INFORMATION

Corresponding Authors

Tomasz Róg − *Department of Physics, Faculty of Science, University of Helsinki, FI-00014 Helsinki, Finland;* orcid.org/0000-0001-6765-7013; Email: tomasz.rog@helsinki.fi, tomasz.rog@gmail.com

Mariusz Kepczynski − *Faculty of Chemistry, Jagiellonian University, 30-387 Kraków, Poland;* orcid.org/0000-0002-7304-6881; Email: kepczyns@chemia.uj.edu.pl

Authors

Chetan Poojari − *Department of Physics, Faculty of Science, University of Helsinki, FI-00014 Helsinki, Finland; Theoretical Physics and Center for Biophysics, Saarland University, 66123 Saarbrücken, Germany;* orcid.org/0000-0001-6575-221X

Agata Zak − *Faculty of Chemistry, Jagiellonian University, 30-387 Kraków, Poland*

Monika Dzieciuch-Rojek − *Faculty of Chemistry, Jagiellonian University, 30-387 Kraków, Poland*

Alex Bunker − *Division of Pharmaceutical Biosciences, Drug Research Program, Faculty of Pharmacy, University of Helsinki, 00014 Helsinki, Finland;* orcid.org/0000-0002-1236-9513

Complete contact information is available at: https://pubs.acs.org/10.1021/acs.jpcb.9b11005

Notes

The authors declare no competing financial interest.

ACKNOWLEDGMENTS

For financial support, we thank the Academy of Finland the Center of Excellence program (Grant 307415 (PC, TR)). CSC-IT Centre for Science (Espoo, Finland; Project tty3995) and the Finnish Grid and Cloud Infrastructure (persistent identifier urn:nbn:fi:research-infras-2016072533) are acknowledged for excellent computational resources.

REFERENCES

(1) Freitas, R. A., Jr. *Nanomedicine Vol. 1: Basic Capabilities*; CRC Press: Boca Raton, FL, 1999.

(2) Bunker, A.; Magarkar, A.; Viitala, T. Rational Design of Liposomal Drug Delivery Systems, a Review: Combined Experimental and Computational Studies of Lipid Membranes, Liposomes and Their PEGylation. *Biochim. Biophys. Acta, Biomembr.* **2016**, *1858* (10), 2334−2352.

(3) Kneidl, B.; Peller, M.; Winter, G.; Lindner, L. H.; Hossann, M. Thermosensitive Liposomal Drug Delivery Systems: State of the Art Review. *Int. J. Nanomed.* **2014**, *9*, 4387−4398.

(4) Alavi, M.; Karimi, N.; Safaei, M. Application of Various Types of Liposomes in Drug Delivery Systems. *Adv. Pharm. Bull.* **2017**, 7 (1), 3−9.

(5) Ali, M. H.; Moghaddam, B.; Kirby, D. J.; Mohammed, A. R.; Perrie, Y. The Role of Lipid Geometry in Designing Liposomes for the Solubilisation of Poorly Water Soluble Drugs. *Int. J. Pharm.* **2013**, *453*, 225−232.

(6) Eloy, J. O.; Claro de Souza, M.; Petrilli, R.; Barcellos, J. P. A.; Lee, R. J.; Marchetti, J. M. Liposomes as Carriers of Hydrophilic Small Molecule Drugs: Strategies to Enhance Encapsulation and Delivery. *Colloids Surf., B* **2014**, *123*, 345−363.
(7) Bulbake, U.; Doppalapudi, S.; Kommineni, N.; Khan, W. Liposomal Formulations in Clinical Use: An Updated Review. *Pharmaceutics* **2017**, *9* (2), 12.
(8) Róg, T.; Pasenkiewicz-Gierula, M.; Vattulainen, I.; Karttunen, M. Ordering Effects of Cholesterol and Its Analogues. *Biochim. Biophys. Acta, Biomembr.* **2009**, *1788* (1), 97−121.
(9) Róg, T.; Vattulainen, I. Cholesterol, Sphingolipids, and Glycolipids: What Do We Know about Their Role in Raft-like Membranes? *Chem. Phys. Lipids* **2014**, *184*, 82−104.
(10) Ohvo-Rekilä, H.; Ramstedt, B.; Leppima, P.; Slotte, J. P. Cholesterol Interactions with Phospholipids in Membranes. *Prog. Lipid Res.* **2002**, *41* (1), 66−97.
(11) Subczynski, W. K.; Pasenkiewicz-Gierula, M.; Widomska, J.; Mainali, L.; Raguz, M. High Cholesterol/Low Cholesterol: Effects in Biological Membranes: A Review. *Cell Biochem. Biophys.* **2017**, *75* (3−4), 369−385.
(12) Berkowitz, M. L. Detailed Molecular Dynamics Simulations of Model Biological Membranes Containing Cholesterol. *Biochim. Biophys. Acta, Biomembr.* **2009**, *1788* (1), 86−96.
(13) Al-Rekabi, Z.; Contera, S. Multifrequency AFM Reveals Lipid Membrane Mechanical Properties and the Effect of Cholesterol in Modulating Viscoelasticity. *Proc. Natl. Acad. Sci. U. S. A.* **2018**, *115* (11), 2658−2663.
(14) Khatibzadeh, N.; Gupta, S.; Farrell, B.; Brownell, W. E.; Anvari, B. Effects of Cholesterol on Nano-Mechanical Properties of the Living Cell Plasma. *Soft Matter* **2012**, *8* (32), 8350−8360.
(15) Khelashvili, G.; Harries, D. How Cholesterol Tilt Modulates the Mechanical Properties of Saturated and Unsaturated Lipid Membranes. *J. Phys. Chem. B* **2013**, *117*, 2411−2421.
(16) Pan, J.; Tristram-Nagle, S.; Nagle, J. F. Effect of Cholesterol on Structural and Mechanical Properties of Membranes Depends on Lipid Chain Saturation. *Phys. Rev. E* **2009**, *80*, 021931.
(17) Shinoda, W. Permeability across Lipid Membranes. *Biochim. Biophys. Acta, Biomembr.* **2016**, *1858* (10), 2254−2265.
(18) Milianta, P. J.; Muzzio, M.; Denver, J.; Cawley, G.; Lee, S. Water Permeability across Symmetric and Asymmetric Droplet Interface Bilayers: Interaction of Cholesterol Sulfate with DPhPC. *Langmuir* **2015**, *31*, 12187−12196.
(19) Issack, B. B.; Peslherbe, G. H. Effects of Cholesterol on the Thermodynamics and Kinetics of Passive Transport of Water through Lipid Membranes. *J. Phys. Chem. B* **2015**, *119* (29), 9391−9400.
(20) Lopez, M.; Denver, J.; Evangelista, S. E.; Armetta, A.; Di Domizio, G.; Lee, S. Effects of Acyl Chain Unsaturation on Activation Energy of Water Permeability across Droplet Bilayers of Homologous Monoglycerides: Role of Cholesterol. *Langmuir* **2018**, *34* (5), 2147−2157.
(21) Dotson, R. J.; Smith, C. R.; Bueche, K.; Angles, G.; Pias, S. C. Influence of Cholesterol on the Oxygen Permeability of Membranes: Insight from Atomistic Simulations. *Biophys. J.* **2017**, *112* (11), 2336−2347.
(22) Saito, H.; Shinoda, W. Cholesterol Effect on Water Permeability through DPPC and PSM Lipid Bilayers: A Molecular Dynamics Study. *J. Phys. Chem. B* **2011**, *115* (51), 15241−15250.
(23) Fujimoto, T.; Parmryd, I. Interleaflet Coupling, Pinning, and Leaflet Asymmetry—Major Players in Plasma Membrane Nanodomain Formation. *Front. Cell Dev. Biol.* **2017**, *4*, 155.
(24) Kulig, W.; Cwiklik, L.; Jurkiewicz, P.; Róg, T.; Vattulainen, I. Cholesterol Oxidation Products and Their Biological Importance. *Chem. Phys. Lipids* **2016**, *199*, 144−160.
(25) Yin, H.; Xu, L.; Porter, N. A. Free Radical Lipid Peroxidation: Mechanisms and Analysis. *Chem. Rev.* **2011**, *111* (10), 5944−5972.
(26) Schrack, S.; Hohl, C.; Schwack, W. Oxysterols in Cosmetics—Determination by Planar Solid Phase Extraction and Gas Chromatography−mass Spectrometry. *J. Chromatogr. A* **2016**, *1473*, 10−18.
(27) Maldonado-Pereira, L.; Schweiss, M.; Barnaba, C.; Medina-Meza, I. G. The Role of Cholesterol Oxidation Products in Food Toxicity. *Food Chem. Toxicol.* **2018**, *118*, 908−939.
(28) Wang, C.; Siriwardane, D. A.; Jiang, W.; Mudalige, T. Quantitative Analysis of Cholesterol Oxidation Products and Desmosterol in Parenteral Liposomal Pharmaceutical Formulations. *Int. J. Pharm.* **2019**, *569*, 118576.
(29) Peeters, J.; Neeskens, P.; Tollenaere, J. P.; Van Remoortere, P.; Brewster, M. E. Characterization of the Interaction of 2-hydroxypropyl-β-cyclodextrin with Itraconazole at PH 2, 4, and 7. *J. Pharm. Sci.* **2002**, *91*, 1414−1422.
(30) Kalepu, S.; Nekkanti, V. Insoluble Drug Delivery Strategies: Review of Recent Advances and Business Prospects. *Acta Pharm. Sin. B* **2015**, *5* (5), 442−453.
(31) Curic, A.; Fricker, G.; Reul, R.; Moschwitzer, J. Formulation Optimization of Itraconazole Loaded PEGylated Liposomes for Parenteral Administration by Using Design of Experiments. *Int. J. Pharm.* **2013**, *448*, 189−197.
(32) Dzieciuch-Rojek, M.; Poojari, C.; Bednar, J.; Bunker, A.; Kozik, B.; Nowakowska, M.; Vattulainen, I.; Wydro, P.; Kepczynski, M.; Róg, T. Effects of Membrane PEGylation on Entry and Location of Antifungal Drug Itraconazole and Their Pharmacological Implications. *Mol. Pharmaceutics* **2017**, *14* (4), 1057−1070.
(33) Kwolek, U.; Kulig, W.; Wydro, P.; Nowakowska, M.; Róg, T.; Kepczynski, M. Effect of Phosphatidic Acid on Biomembrane: Experimental and Molecular Dynamics Simulations Study. *J. Phys. Chem. B* **2015**, *119* (31), 10042−10051.
(34) Kepczynski, M.; Kumorek, M.; Stepniewski, M.; Róg, T.; Kozik, B.; Jamróz, D.; Bednar, J.; Nowakowska, M. Behavior of 2,6-Bis(Decyloxy)Naphthalene inside Lipid Bilayer. *J. Phys. Chem. B* **2010**, *114* (47), 15483−15494.
(35) Kepczynski, M.; Ehrenberg, B. Interaction of Dicarboxylic Metalloporphyrins with Liposomes The Effect of PH on Membrane Binding Revisited. *Photochem. Photobiol.* **2002**, *76* (76), 486−492.
(36) Jorgensen, W. L.; Maxwell, D. S.; Tirado-Rives, J. Development and Testing of the OPLS All-Atom Force Field on Conformational Energetics and Properties of Organic Liquids. *J. Am. Chem. Soc.* **1996**, *118* (45), 11225−11236.
(37) Kaminski, G. A.; Friesner, R. A.; Tirado-Rives, J.; Jorgensen, W. L. Evaluation and Reparametrization of the OPLS-AA Force Field for Proteins via Comparison with Accurate Quantum Chemical Calculations on Peptides. *J. Phys. Chem. B* **2001**, *105* (28), 6474−6487.
(38) Fischer, N. M.; Van Maaren, P. J.; Ditz, J. C.; Yildirim, A.; Van Der Spoel, D. Properties of Organic Liquids When Simulated with Long-Range Lennard-Jones Interactions. *J. Chem. Theory Comput.* **2015**, *11* (7), 2938−2944.
(39) Kulig, W.; Pasenkiewicz-Gierula, M.; Róg, T. Cis and Trans Unsaturated Phosphatidylcholine Bilayers: A Molecular Dynamics Simulation Study. *Chem. Phys. Lipids* **2016**, *195*, 12−20.
(40) Kulig, W.; Pasenkiewicz-Gierula, M.; Róg, T. Topologies, Structures and Parameter Files for Lipid Simulations in GROMACS with the OPLS-Aa Force Field: DPPC, POPC, DOPC, PEPC, and Cholesterol. *Data Br.* **2015**, *5*, 333−336.
(41) Maciejewski, A.; Pasenkiewicz-Gierula, M.; Cramariuc, O.; Vattulainen, I.; Róg, T. Refined OPLS-AA Force Field for Saturated Phosphatidylcholine Bilayers at Full Hydration. *J. Phys. Chem. B* **2014**, *118* (17), 4571−4581.
(42) Harder, E.; Damm, W.; Maple, J.; Wu, C.; Reboul, M.; Xiang, J. Y.; Wang, L.; Lupyan, D.; Dahlgren, M. K.; Knight, J. L.; et al. OPLS3: A Force Field Providing Broad Coverage of Drug-like Small Molecules and Proteins. *J. Chem. Theory Comput.* **2016**, *12* (1), 281−296.
(43) Jorgensen, W. L.; Chandrasekhar, J.; Madura, J. D.; Impey, R. W.; Klein, M. L. Comparison of Simple Potential Functions for Simulating Liquid Water. *J. Chem. Phys.* **1983**, *79* (2), 926−935.
(44) Abraham, M. J.; Murtola, T.; Schulz, R.; Páll, S.; Smith, J. C.; Hess, B.; Lindahl, E. Gromacs: High Performance Molecular

https://dx.doi.org/10.1021/acs.jpcb.9b11005
J. Phys. Chem. B 2020, 124, 2139−2148

Simulations through Multi-Level Parallelism from Laptops to Supercomputers. *SoftwareX* **2015**, *1*−*2*, 19−25.
(45) Hess, B.; Bekker, H.; Berendsen, H. J. C.; Fraaije, J. G. E. M. LINCS: A Linear Constraint Solver for Molecular Simulations. *J. Comput. Chem.* **1997**, *18* (12), 1463−1472.
(46) Hoover, W. G. Canonical Dynamics: Equilibrium Phase-Space Distributions. *Phys. Rev. A: At., Mol., Opt. Phys.* **1985**, *31* (3), 1695−1697.
(47) Nosé, S. A Unified Formulation of the Constant Temperature Molecular Dynamics Methods. *J. Chem. Phys.* **1984**, *81* (1), 511−519.
(48) Parrinello, M.; Rahman, A. Polymorphic Transitions in Single-Crystals - A New Molecular-Dynamics Method. *J. Appl. Phys.* **1981**, *52* (12), 7182−7190.
(49) Essmann, U.; Perera, L.; Berkowitz, M. L.; Darden, T.; Lee, H.; Pedersen, L. G. A Smooth Particle Mesh Ewald Method. *J. Chem. Phys.* **1995**, *103* (19), 8577−8593.
(50) Darden, T.; York, D.; Pedersen, L. Particle Mesh Ewald: An *N*·log(*N*) Method for Ewald Sums in Large Systems. *J. Chem. Phys.* **1993**, *98* (12), 10089−10092.
(51) Humphrey, W.; Dalke, A.; Schulten, K. VMD-Visual Molecular Dynamics. *J. Mol. Graphics* **1996**, *14*, 33−38.
(52) Jurak, M. Thermodynamic Aspects of Cholesterol Effect on Properties of Phospholipid Monolayers: Langmuir and Langmuir-Blodgett Monolayer Study. *J. Phys. Chem. B* **2013**, *117* (13), 3496−3502.
(53) Wydro, P.; Knapczyk, S.; Łapczyńska, M. Variations in the Condensing Effect of Cholesterol on Saturated versus Unsaturated Phosphatidylcholines at Low and High Sterol Concentration. *Langmuir* **2011**, *27* (9), 5433−5444.
(54) Kepczyński, M.; Nawalany, K.; Kumorek, M.; Kobierska, A.; Jachimska, B.; Nowakowska, M. Which Physical and Structural Factors of Liposome Carriers Control Their Drug-Loading Efficiency? *Chem. Phys. Lipids* **2008**, *155* (1), 7−15.

https://dx.doi.org/10.1021/acs.jpcb.9b11005
J. Phys. Chem. B 2020, 124, 2139−2148